Rare Metal Materials and Engineering
Volume 51, Issue 1, January 2022
Available online at www.rmme.ac.cn

Science Press

Cite this article as: Yan Huajin, Tian Sugui, Dong Zhifeng. Deformation and Damage Behavior of Single Crystal Nickel-based Superalloy During Elevated Temperature Creep[J]. Rare Metal Materials and Engineering, 2022, 51(01): 44-51.

ARTICLE

Deformation and Damage Behavior of Single Crystal Nickel-based Superalloy During Elevated Temperature Creep

Yan Huajin[1,3], Tian Sugui[2], Dong Zhifeng[1]

[1] School of Mechanical Electronic & Information Engineering, China University of Mining and Technology-Beijing, Beijing 100083, China; [2] School of Materials Science and Engineering, Shenyang University of Technology, Shenyang 110870, China; [3] School of Mechanical Engineering, Guizhou University of Engineering Science, Bijie 551700, China

Abstract: The deformation and damage behavior of the single crystal Ni-based alloy during elevated temperature creep were investigated through analyzing creep properties and microstructure. The results show that the creep life of Ni alloy under the condition of 1040 °C/137 MPa is 556 h, displaying an excellent creep resistance of Ni alloy. The creep feature of Ni alloy at steady state is the dislocation glide in γ phase and dislocation climb over the γ' rafts. In the late stage of creep, the deformation feature of Ni alloy is that the γ' rafts are sheared by the dislocations of cross-slip, which forms the Kear-Wilsdorf (K-W) locks to restrain the dislocation glide and cross-slip dislocation. The cross-slip dislocations cause the distortion of γ/γ' rafts, thereby promoting the initiation of cracks along the γ'/γ interfaces and the interface fracture, which is the damage and fracture features of Ni alloy. The condition of $\sigma > \eta/\alpha$ is considered as the prerequisite for unstable crack propagation.

Key words: single crystal Ni-based alloy; microstructure; creep; deformation mechanism; damage feature

Because of the excellent mechanical and creep properties under high-temperature service conditions, the single crystal Ni-based alloys are widely applied for production of blade parts of advanced aero-engine and industrial gas engine[1-3]. The temperature endurance of the heat-resistance parts in aero-engine needs to be further improved with the enhancement of the aero-engine power.

Adding Re may enhance the temperature endurance of alloys. The feature of the second-generation and the third-generation Ni-based alloys is their composition with 3wt% and 6wt% Re, respectively[4]. However, adding excess Re may increase the manufacturing cost, decrease the microstructure stability, and promote the precipitation of topologically close-packed (TCP) phase under service condition at high temperature[5], which restricts the extensive use of Re-containing single crystal alloys. Therefore, it is necessary to develop a Re-free Ni-based alloy with high creep resistance on the premise of retaining the excellent properties of the second-generation single crystal alloy, which can reduce the manufacturing cost and restrain the precipitation of TCP phase. According to Ref. [6-8], the strength and creep resistance of alloys can be improved by adding the refractory elements. Particularly, the Mo addition in the Re-free alloys is mainly distributed in the γ phase, and the γ phase is enhanced with increasing the Mo content, which can ameliorate the performance of alloys at high temperature.

Despite the excellent properties of single crystal alloys with high alloying extent under service conditions, the creep damage is still the main failure mode[9-11]. Thus, the creep and damage features of single crystal Ni-based alloys are widely studied. In the late creep period, the deformation mechanism of alloys under medium temperature is that the γ'/γ phases are sheared by dislocations. In particular, the cross-slip dislocation causes the distortion of γ/γ' phases so that some cracks and holes appear in the interfaces of γ/γ' phases[12-14]. According to Ref. [15, 16], the anomalous yield behavior of Ni_3Al single crystal at 650~700 °C is attributed to the creep dislocations with cross slip from {111} plane to {100} plane

Received date: May 21, 2021
Foundation item: National Natural Science Foundation of China (51271125); Sponsored by Guizhou Province (KY[2019]053, KY[2019]155, KY[2019]156, [2020]1Y198, G[2019]9, [2019]2)
Corresponding author: Tian Sugui, Ph. D., Professor, School of Materials Science and Engineering, Shenyang University of Technology, Shenyang 110870, P. R. China, Tel: 0086-10-62331370, E-mail: yanhuajin317@163.com

to form the Kear-Wilsdorf (K-W) locks, which may restrain the dislocation glide and cross-slip dislocation. Moreover, as the creep process continues, some cracks are initiated and expanded along the γ/γ' interfaces which are vertical to stress axis until rupture. These phenomena are the damage and fracture features of alloys during creep process[17].

During creep at high temperature, the γ' phase in alloy changes into the raft configuration, which can impede the dislocation movement[18]. Therefore, the dislocation climb over the γ' rafts is considered as the restriction condition to creep. Besides, the Re-free alloy may maintain the excellent mechanical properties at high temperature. However, it is not clear whether K-W locks are formed during the creep of alloy at 1040 °C, and the initiation and propagation features of the cracks during creep at high temperature need to be further investigated.

In this research, the Re-free single crystal Ni-based alloy was prepared. The creep behavior of Re-free single crystal Ni-based alloy at high temperature was investigated to explore the damage and fracture features of the alloy during elevated temperature creep through analyses of creep properties and microstructure.

1 Experiment

The Re-free single crystal Ni-based alloys with [001] direction were prepared in a directional solidifying vacuum furnace under high temperature gradient by selecting crystal method. The experiment alloy was Ni-Al-7Ta-Cr-Co-4W-6Mo (mass fraction). Based on Laue back reflection method, all the orientations had the difference in orientation deviating from the [001] direction within 7°. Three sections of heat treatments were conducted in the following order: (1) 1280 °C/2 h+1300 °C/2 h+1315 °C/6 h+air cooling; (2) 1080 °C/4 h+air cooling; (3) 870 °C/24 h+air cooling. In addition, the γ and γ' phases in the alloy had the negative lattice misfits.

After the heat treatment, the single crystal alloys were processed into creep specimens with the cross-section of 4.5 mm×2.5 mm and the gauge length of 20 mm on the (100) plane along [001] direction. After mechanical grinding and polishing, the creep properties of the specimens under various conditions were measured by the creep test machine with GTW504 model.

For the ground and polished specimens at different states, the solution of 20 g $CuSO_4$+5 mL H_2SO_4+100 mL HCl+80 mL H_2O was used for chemical corrosion. Then, the scanning electron microscope (SEM) of S3400 model was used to observe the morphology of alloys at different states. The films with the diameter of 3 mm and the thickness of 60 μm were prepared by grinding and polishing the specimens after creep for different durations. The specimens were thinned using the electrolyte with 7vol% perchloric acid and 93vol% ethanol by twin-jet polishing technique at 253 K. Then the morphology of alloys during creep was observed by the transmission electron microscope (TEM) of TECNA120 model. The creep mechanism at high temperature was also analyzed.

2 Results

2.1 Creep behavior

The creep curves of Re-free alloys under different conditions are in Fig. 1. Fig. 1a shows that the strain rate is increased firstly and then decreased during the creep process. The creep of alloys enters into the steady stage when the strain rate decreases to the minimum value. According to the slope of curves, the strain rate of alloys at steady state creep at 1040, 1060, and 1070 °C is 0.0034%/h, 0.0085%/h and 0.0139%/h, and the creep life of Ni-based alloy of alloys is 556, 335, and 239 h, respectively. The creep life of Ni-based alloy at 1060 °C is decreased by approximate 40% than that at 1040 ° C, indicating that the Ni-based alloy is sensitive to the applied temperature over 1040°C under stress of 137 MPa.

Fig.1b shows that the alloys under the applied stress of 137 MPa display a lower strain rate during steady state creep. The creep life of alloys after 200 h is still in the steady state stage. The creep life and strain rate of alloys under 147 MPa are 180 h and 0.014%/h, respectively. When the applied stress changes to 160 MPa, the creep life and strain rate are 110 h and 0.0316%/h, respectively.

In a flash of applying temperature and loading, the larger instantaneous strain and strain rate exist in the primary creep period of alloys with many activated dislocations in γ phase. Then, under the deformation strengthening, the strain rate is reduced and the creep enters into the steady state. The alloy

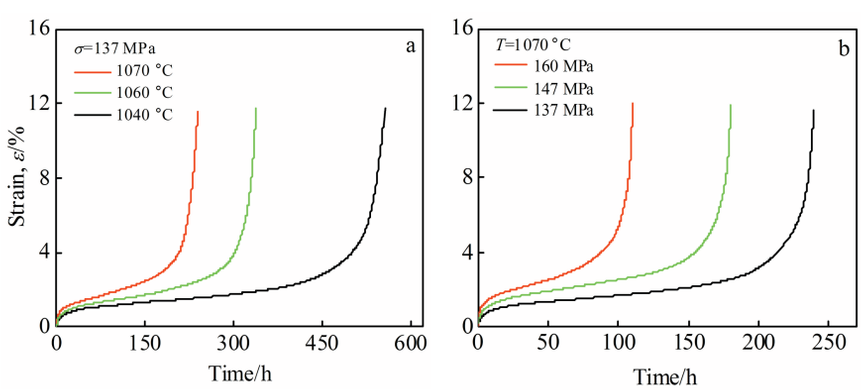

Fig.1 Creep curves of Ni-based alloys under stress of 137 MPa at different temperatures (a) and under different stresses at 1070 °C (b)

maintains a constant strain rate, as described by Norton law, as follows:

$$\dot{\varepsilon}_{ss} = A\sigma_A^n \exp\left(-\frac{Q}{RT}\right) \quad (1)$$

where A refers to a constant related to the structure, T means the thermodynamics temperature, R means the gas constant, Q stands for the creep activation energy, n means the stress exponent, and σ_A represents the applied stress. The strain rate of the alloys during steady state creep can be calculated according to the data in Fig. 1. Thus, the relationship between the strain rate and the temperatures and that between the strain rate and stress can be expressed as $\ln\dot{\varepsilon}_{ss}$-$T^{-1}$ and $\ln\dot{\varepsilon}_{ss}$-$\ln\sigma$, respectively. The creep activation energy and stress exponent of alloys during steady state creep can be calculated as Q= 486.5 kJ/mol and n=4.8, respectively. It can be concluded that the deformation mechanism of Ni-based alloys during steady state creep is the dislocation slip in γ matrix and the dislocation climb over γ' rafts, because the stress exponent n is 4.8, which is between 3 and 6[19].

2.2 Microstructure during creep

After the heat treatment, the cuboidal γ' phase in Ni-based alloys is embedded into the γ matrix and arranged regularly along the <100> direction, and the alloy morphology of (001) plane is shown in Fig. 2. The mean dimension of the cuboidal γ' phase and the width of γ channels are about 0.45 and 0.1 μm, respectively, and the fraction of γ' phase is approximately 65.0vol%.

After the creep and rupture at 1040 °C/137 MPa, the surface morphologies of different areas of Ni-based alloys are displayed in Fig. 3. The γ' precipitates in the area B are transformed into the raft structure, and the thickness of γ' rafts is about 0.5 μm. However, some tiny γ phases still exist in the γ' rafts along the direction parallel to the stress axis, as indicated by the arrow in Fig. 3b. Thus, the γ' precipitates in this area are only transformed into an incomplete raft structure. Although most γ' precipitates in the area C are transformed into the raft structure, some fine γ phases still exist, as indicated by the arrow in Fig.3c.

In the area D in Fig. 3d, the γ' phase in alloy is fully transformed into the raft structure. Compared with the structures in area C, the γ' rafts in the area D are distorted and broken, displaying the block-like configuration, as indicated by the arrows in Fig. 3d. But the large plastic deformation leads to the coarsening and distortion of γ' rafts in the area E, as shown in Fig.3e. The thickness of γ' rafts is increased to 0.7 μm, whereas the length of γ' rafts is reduced, because the γ' rafts are twisted and broken by the large plastic deformation in the necking area. The inclined angle between the twisted γ' rafts and stress axis is about 45°, as shown in Fig.3e.

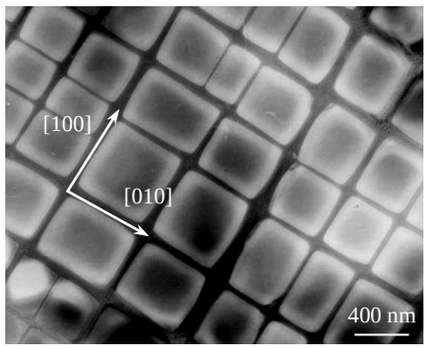

Fig.2 Microstructure of (001) plane in Ni-based alloys after heat treatment

2.3 Deformation characteristics during creep

The morphologies of Ni-based alloys after creep at 1040 °C/137 MPa for different durations are displayed in Fig.4, and the directions of applied loading are marked by the arrows. The operating vector $\boldsymbol{g}$=[002] is also marked in it. Fig.4a indicates that after creep for 10 h, a few γ' rafts are formed in the alloys. Plenty of dislocations glide and cross-slip dislocations in γ phase occur, and the twisted dislocations are distributed in the area A. Some dislocations even display the feature with 90° fold line, as labeled by the arrow in Fig.4a.

Fig. 4b shows that after creep for 50 h, the γ' phase is transformed into the raft structure, and the dislocation networks are distributed in γ'/γ interfaces[20]. Some dislocations in γ matrix are distributed in the area B, but a few dislocations can be observed in γ'-Ni_3Al phase.

Fig.4c shows that after creep for 300 h, the γ' rafts in the Ni-

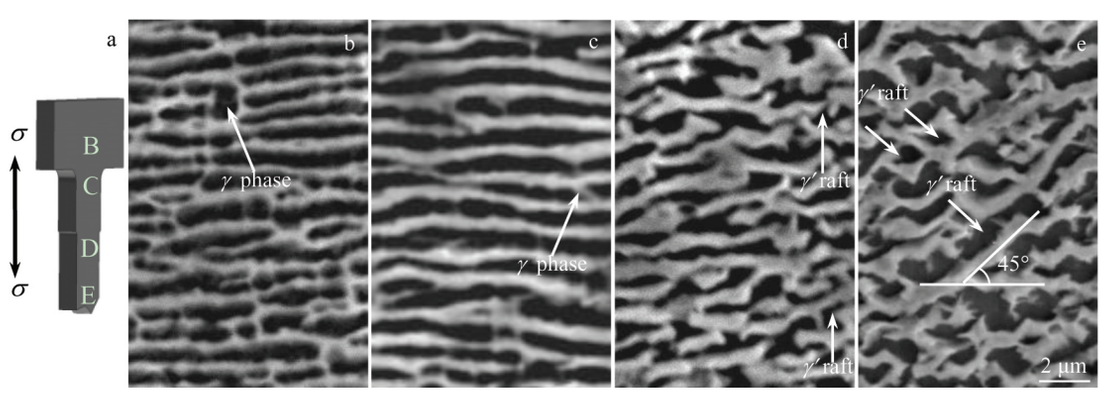

Fig.3 Schematic diagram (a) and surface morphologies (b~e) of different areas of Ni-based alloys after creep for 556 h and rupture at 1040 °C/137 MPa: (b) area B, (c) area C, (d) area D, and (e) area E in Fig.3a

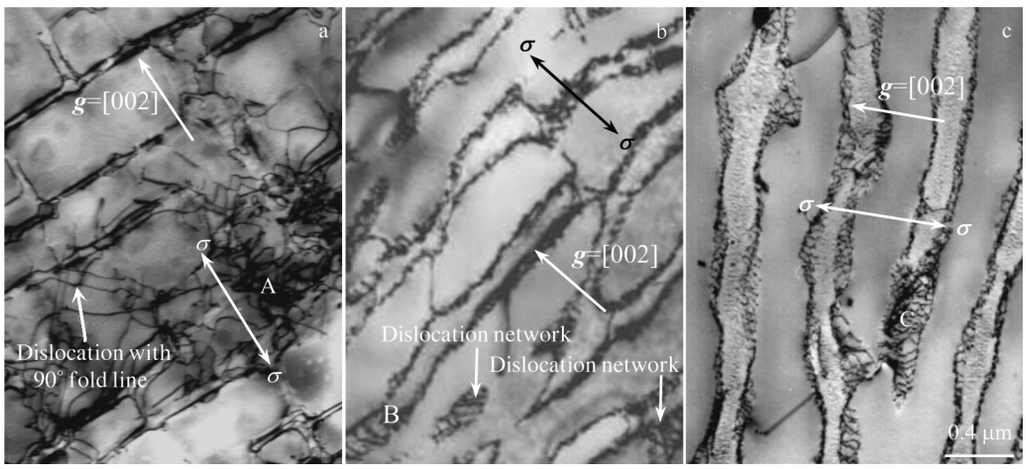

Fig.4 Morphologies of Ni-based alloys after creep at 1040 °C/137 MPa for 10 h (a), 50 h (b), and 300 h (c)

based alloys display a smooth and layered configuration, because the creep of alloy is still in the steady state period. In addition, the thickness of γ matrix is about 0.2 μm, and the denser dislocation networks are distributed in the γ'/γ interfaces, as shown in the area C in Fig. 4c. A few dislocations can be observed in the γ' rafts, indicating that this area of alloy still has the excellent creep resistance.

The microstructure of Ni-based alloys after creep at 1040 °C/137 MPa for 350 h is displayed in Fig. 5, which corresponds to the steady state stage of the creep curve in Fig. 1a. It can be seen that the γ' phase in Ni-based alloys still maintains the raft structure, and some dislocation networks are distributed in γ'/γ interfaces, as marked by the rectangle area and the arrow. The magnified morphology in Fig. 5 shows the denser dislocation glide in γ matrix. However, a few dislocations are observed in γ' phase, and the γ' rafts are sheared by dislocations, which indicates that the deformation mechanisms of Ni-based alloys during steady state creep are dislocation glide in γ matrix and dislocation climb over the γ' rafts, because the strain of Ni-based alloys after creep for 350 h is about 2%, as shown in Fig. 1a.

Based on the analysis, it is considered that the dislocations in γ matrix glide to the interface to react with the dislocation networks, which may alter the direction of dislocation movement[21,22], thereby promoting the dislocation climb. Consequently, it can be concluded that the dislocation networks in the interface play a coordinated role in the deformation strengthening and recovery softening in alloys during the steady state creep[7], which may delay the stress concentration and dislocations shearing of γ/γ' rafts.

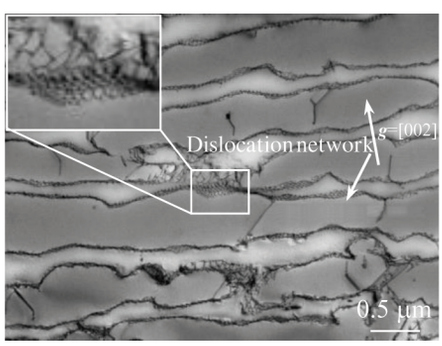

Fig.5 Morphology of Ni-based alloy after creep at 1040 °C/137 MPa for 350 h

2.4 Creep damage

After creep at 1040 °C/137 MPa for 556 h and fracture, the microstructures in different areas of Ni-based alloys are shown in Fig. 6. Fig. 6a shows that in the area far away from the fracture area, the γ' phase still remains the raft structure. The morphology of γ' phase sheared by dislocations is shown in the area A of Fig. 6a.

Fig. 6b shows that some shear dislocations in the area beside the fracture zone are located in the area C. A great deal of shear dislocations may cause the crystal rotation to produce the orientation difference[23], thereby displaying a dark contrast of the γ' rafts in the area D in Fig. 6b.

Fig. 6c shows that in another area near the fracture zone, the distortion of γ/γ' rafts is aggravated (area E). A large number of cross slip dislocations in γ matrix moving to the interface of γ' rafts are hindered, which may cause the stress concentration. The stress concentration is increased with proceeding the creep process. On the one hand, the stress concentration may damage the dislocation networks of γ'/γ interface; on the other hand, the γ' phase may be sheared by the dislocations in γ matrix from the area of damaged networks. Moreover, those dislocations may cause the cross-slip to form the fold line feature, as shown in Fig. 6c. The dislocation glide may occur in γ matrix, as shown in the area F in Fig. 6c, and the traces of dislocation glide in γ matrix are about at 45° to the stress axis. In addition, the denser networks in γ/γ' interfaces can be observed in the area G in Fig. 6c. Some shear dislocations indicate that the area of Ni-based alloys does not retain the creep resistance, so the γ' rafts are sheared by dislocations to accelerate the creep process until fracture.

The dislocation configurations of Ni-based alloys after

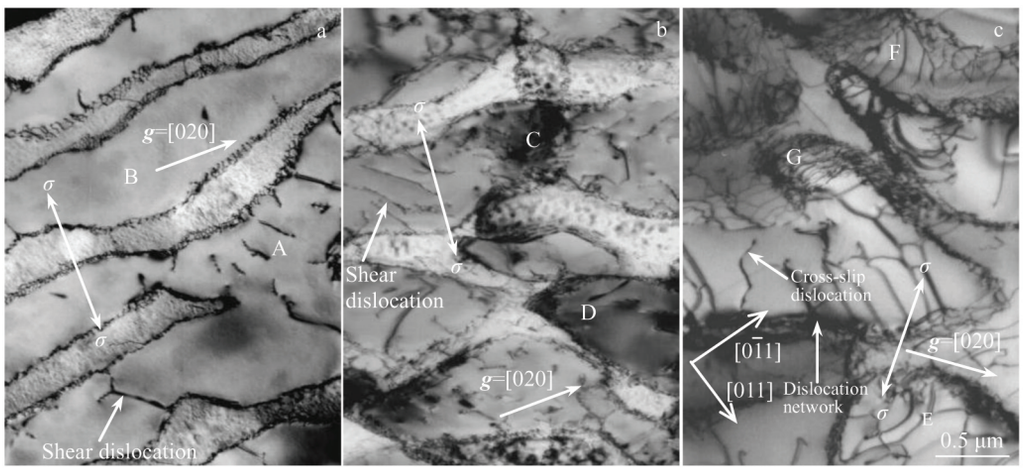

Fig.6 Deformation morphologies of different areas of Ni-based alloys after creep at 1040 °C/137 MPa for 556 h and fracture: (a) far away from fracture; (b) beside fracture; (c) other area near fracture

creep and rupture at 1040 °C/137 MPa are shown in Fig. 7. Some dislocation networks in γ/γ' interface are damaged to form the twisted dislocations, as marked by the arrow and region C in Fig. 7a. It can be seen that the γ' phase is sheared by two sets of dislocations with different configurations. The dislocations with double lines and dark contrast are marked by A, and the ones with single line and long features are marked by B in Fig. 7a. The dislocations A and B exhibit contrast under the operating vector of $\boldsymbol{g}=[1\bar{1}\bar{1}]$, as shown in Fig. 7a. But the dislocation A disappears under the operating vector of $\boldsymbol{g}=[02\bar{2}]$ and $\boldsymbol{g}=[\bar{1}1\bar{1}]$, as shown in Fig. 7b and 7d, respectively. According to the Burgers vector of dislocation A, $\boldsymbol{b}_A=\boldsymbol{g}_{[02\bar{2}]}\times\boldsymbol{g}_{[\bar{1}1\bar{1}]}$, it can be transferred into $\boldsymbol{b}_A=1/2[011]$. Because the trace of dislocation A is parallel to $\boldsymbol{g}=[020]$, namely, $\boldsymbol{\mu}_A=[020]$, the dislocation glide plane of dislocation A is defined as $\boldsymbol{b}_A\times\boldsymbol{\mu}_A=(100)$.

Because the γ and γ' phases in the single crystal alloy possess the face centered cubic (fcc) structure, the activated dislocations during creep firstly glide into the {111} plane. When the dislocation glide on {111} plane is hindered, the cross-slip dislocations from {111} plane to {100} plane occur to form the K-W locks with non-plane core structure. Consequently, the dislocations in (100) plane of Ni-based alloys originate from the cross-slip dislocations, and the K-W locks may restrain the dislocation glide and cross-slip dislocation to increase the creep resistance of alloys.

Furthermore, the dislocation A displays the double line contrast due to its decomposition, and the anti-phase boundary (APB) can be observed. The decomposition reaction of dislocation A is $[011]\rightarrow(1/2)[011]+(APB)_{(100)}+(1/2)[011]$.

The dislocation B can be observed under the operating vectors of $\boldsymbol{g}=[020]$ and $\boldsymbol{g}=[\bar{1}1\bar{1}]$, as shown in Fig. 7c and 7d, respectively. Thus, the dislocation B in Ni-based alloys is identified as the super-dislocation with the Burgers vector of $\boldsymbol{b}_B=[10\bar{1}]$. Because the trace of dislocation B is parallel to $\boldsymbol{g}=[022]$, namely, $\boldsymbol{\mu}_B=[022]$, the dislocation glide plane of dislocation B is $\boldsymbol{b}_B\times\boldsymbol{\mu}_B=(11\bar{1})$. The deformation mechanism of Ni-based alloys in the late creep period is that the γ' rafts are sheared by the <110> super-dislocations, and the shear dislocations may glide on both the {111} and {100} planes. In

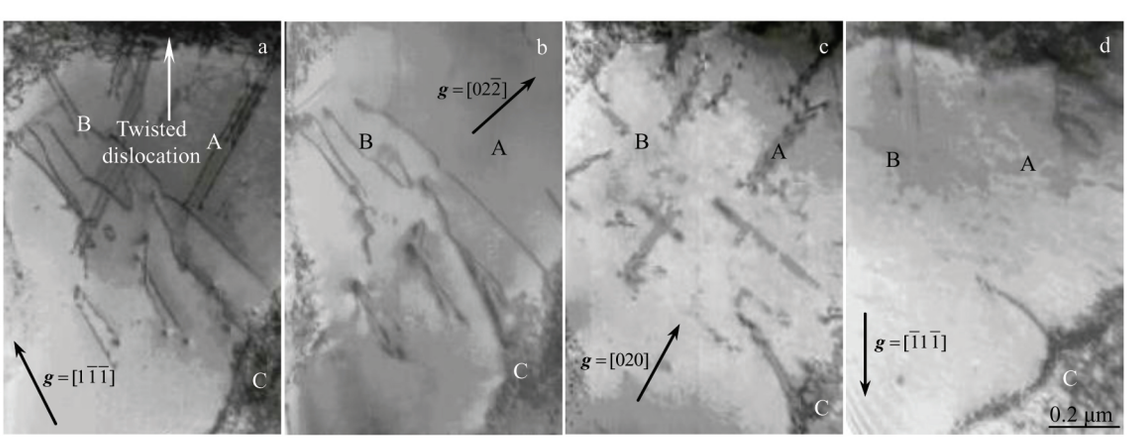

Fig.7 Dislocation configurations of Ni-based alloys after creep at 1040 °C/137 MPa and rupture based on different operating vectors: (a) $\boldsymbol{g}=[1\bar{1}\bar{1}]$, $\boldsymbol{B}=[110]$; (b) $\boldsymbol{g}=[02\bar{2}]$, $\boldsymbol{B}=[110]$; (c) $\boldsymbol{g}=[020]$, $\boldsymbol{B}=[100]$; (d) $\boldsymbol{g}=[\bar{1}1\bar{1}]$, $\boldsymbol{B}=[110]$

addition, APB is formed by decomposing the shear dislocations to enhance the creep resistance of alloys.

Microstructure observation indicates that the deformation mechanisms in the late creep period are the dislocation glide in γ matrix and the γ' rafts sheared by dislocations. With proceeding the creep process, the γ and γ' phases are alternately sheared by the initial/secondary dislocation glide due to the orientation difference. The γ and γ' phases are firstly sheared by the initial gliding dislocation, and then sheared by the activated secondary gliding dislocation, which leads to the distortion of γ'/γ rafts. Meanwhile, the strain of alloys is increased with proceeding the creep process to aggravate the distortion of γ' rafts, which may promote the initiation and expansion of cracks along the γ'/γ interfaces until fracture. These phenomena are the deformation and damage features of Ni-based alloys in the late creep stage.

After creep at 1040 °C/137 MPa and rupture, the morphologies of the crack are shown in Fig.8. Lots of dislocations in γ matrix gliding to the interfaces of γ' phase are blocked to generate the stress concentration in the late creep stage. The stress concentration is increased with proceeding the creep process, which may damage the dislocation networks in the γ/γ' interfaces[22,24]. Then the γ' phase in the interfaces of damaged networks may be sheared by dislocations. The initial and secondary dislocation glides cause the distortion of γ' rafts, which promotes the formation of cracks and micro-holes in γ/γ' interfaces, as shown in the zone A of Fig.8a.

In the late creep period, the micro-cracks are formed in the interfaces of γ/γ' rafts. With proceeding the creep process, the micro-cracks in other areas near the fracture are expanded in γ/γ' interfaces along the direction which is vertical to the stress axis, as shown in the area B of Fig. 8b. With further proceeding the creep process, the stress concentration occurs again in crack tip, which promotes the crack propagation along the interface. Due to the crack propagation, a larger crack along the interfaces near the fracture can be observed in Fig. 8c. With further proceeding the creep process, the large cracks on different cross-sections are connected by tearing edges until fracture, which is the rupture characteristic of Ni-based alloys in the late creep stage at elevated temperatures[25].

3 Discussion

Based on the microstructure observation, the γ' phase being sheared by dislocations is considered as the deformation mechanism of Ni-based alloy in the late creep period. The initial and secondary dislocation glides cause the distortion of γ'/γ rafts, which promotes the crack initiation and propagation along γ/γ' interfaces. The schematic diagrams of the initial/secondary dislocation glide on the (100) plane are shown in Fig.9.

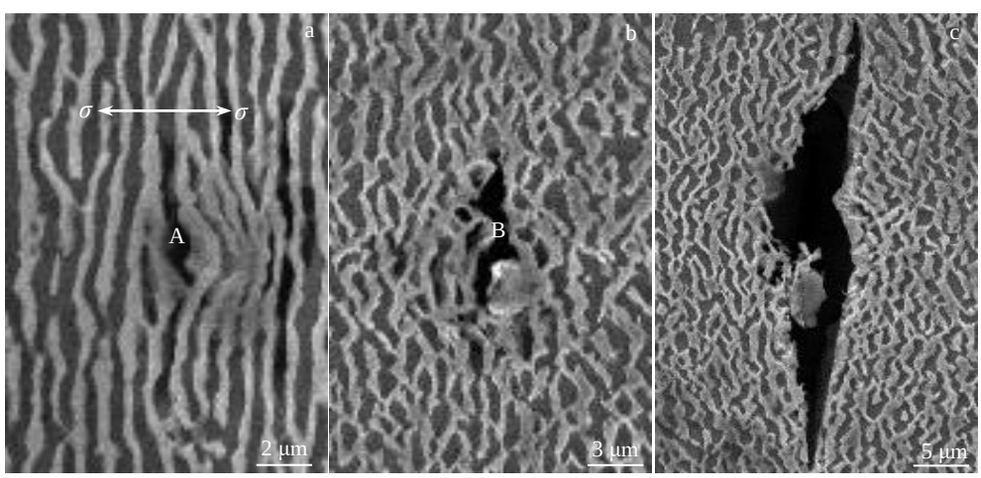

Fig.8 Morphologies of Ni-based alloys after creep at 1040 °C/137 MPa for 556 h and rupture in the area beside fracture zone: (a) crack initiation, (b) crack propagation, and (c) crack expansion

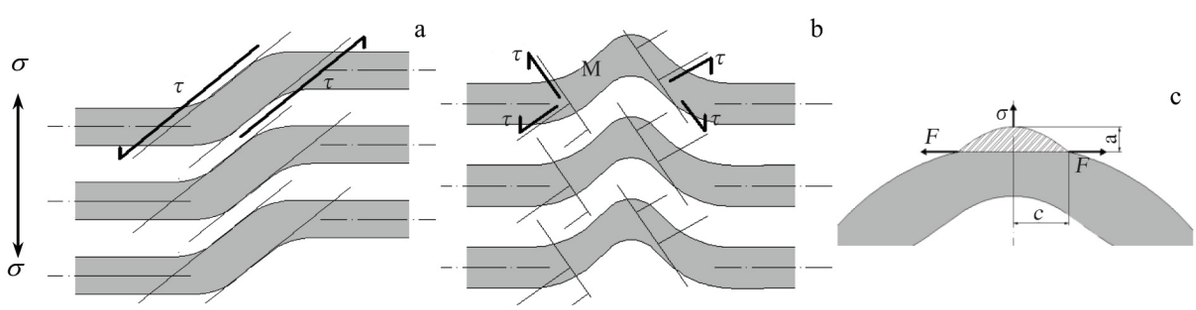

Fig.9 Schematic diagrams of initial (a) and secondary (b) dislocation glides for crack initiation and propagation; schematic diagram of crack (c)

The dark zones in Fig. 9 stand for the γ' rafts in Ni-based alloys, and the white area represents the γ matrix. In the late creep period, the dislocation glide is firstly activated under the maximum shear stress, which causes the distortion of γ'/γ rafts along the direction about 45° to the [001] direction (Fig. 9a). With proceeding the creep process, the activated secondary dislocation glide causes the twist of γ'/γ rafts along the other direction of the maximum shear stress, resulting in the fact that the original γ'/γ rafts are transformed into the distorted configurations with the inverted V-like feature on the (100) plane, as shown in Fig.3e and Fig.9b. Moreover, a larger stress concentration occurs in the bulge of γ/γ' interface due to the activation of initial/secondary dislocation glide, resulting in the appearance of the micro-holes in the bulge area, as indicated by the area M in Fig.9b.

With further proceeding the creep process, the micro-cracks are formed by accumulation of micro-holes, leading to the crack propagation along the interface. As shown in Fig.9c, the formed micro-crack is indicated by the gray area, a is the crack displacement along the stress axis direction, and $2c$ is the crack length. With further proceeding the creep process, the tension stress is generated at the tip area of micro-crack, as indicated by the letter F in Fig. 9c, resulting in the stress concentration. With increasing the stress concentration, the crack expansion along the direction vertical to applied loading occurs until creep rupture.

Because the stability of the crack formation is related to the energy, the free energy change for forming the crack with length of $2c$ and displacement of a under the plane-strain condition can be expressed as follows:

$$\Delta G=\frac{\mu a^2}{4\pi(1-\nu)}\ln\left(\frac{2L}{c}\right)+2\eta c-\frac{\pi(1-\nu)\sigma^2c^2}{2\mu}-\sigma ac \quad (2)$$

where μ stands for the shear modulus, ν means the Poisson's ratio, η *is* the given surface energy, L is the average spacing between the two γ' strengthening phases, and σ represents the applied stress. Based on $\partial\Delta G/\partial c$=0, the minimum length c, namely critical size of crack c_c, of the stable crack is determined as follows:

$$c_c=\frac{\mu\eta}{\pi(1-\nu)\sigma^2}\left[(1-\frac{\sigma\alpha}{2\eta})\pm(1-\frac{\sigma\alpha}{\eta})^{1/2}\right] \quad (3)$$

where α *is* force constant. Because the distortion of γ'/γ rafts and the crack initiation are attributed to the cross-slip dislocations, based on Eq. (3), the crack may be propagated until the creep rupture, i. e., the rupture occurs under the condition of $\sigma>\eta/\alpha$. Therefore, the critical size (c_c) of the crack is confirmed as follows:

$$c_c=\frac{\mu a^2}{2\pi(1-\nu)\eta}=K\frac{a^2}{\eta} \quad (4)$$

According to Eq. (4), the critical size (c_c) of the crack for unstable propagation during creep is proportional to the ratio of the square of crack displacement (a) and the specific surface energy (η). Thus, the condition for unstable crack propagation is obtained. The damage and fracture features of Ni-based alloys in the late creep period are that the initial and secondary dislocation glides cause the distortion of γ' rafts, thereby promoting the crack initiation and propagation until fracture.

4 Conclusions

1) The creep life of the Re-free single crystal Ni-based alloys at 1040 °C/137 MPa is 556 h, displaying the excellent creep resistance.

2) The creep feature of Ni-based alloys during the steady state creep is the dislocation glide in γ phase and dislocation climb over the γ' rafts. The deformation mechanism in the late creep period of Ni-based alloys at 1040 °C is that the γ' rafts are sheared by dislocations which may cause cross-slip dislocation to form the Kear-Wilsdorf locks. The anti-phase boundary originating from the dislocations decomposes, leading to the hindrance of dislocation glide and cross-slip dislocation, thereby enhancing the creep resistance of Ni-based alloys.

3) In the late creep stage, the cross-slip dislocation causes the distortion of γ/γ' rafts, promoting the crack initiation and propagation along interfaces, which is also the damage and fracture features of Ni-based alloys in the late period of creep. The condition of $\sigma>\eta/\alpha$ is the prerequisite of unstable crack propagation.

Reference

1 Kamaraj M, Radhakrishnan V M. *Transactions of the Indian Institute of Metals*[J], 2017, 70(10): 2485

2 Kim K H, Withey P A. *Advanced Engineering Materials*[J], 2017, 19(6): 1 700 041

3 Chen J B, Chen J Y, Hui X D *et al*. *Rare Metal Materials and Engineering*[J], 2020, 49(7): 2207

4 Montakhab M, Balikci E. *Metallurgical and Materials Transactions A*[J], 2019, 50(7): 3330

5 Volek A, Pyczak F, Singer R F *et al*. *Scripta Materialia*[J], 2005, 52(2): 141

6 Pröbstle M, Neumeier S, Feldner P *et al*. *Materials Science and Engineering A*[J], 2016, 676: 411

7 Yu H, Xu W, Van Der Zwaag S *et al*. *Journal of Materials Science and Technology*[J], 2020, 45(10): 207

8 Xia W S, Zhao X B, Yue L *et al*. *Journal of Materials Science and Technology*[J], 2020, 44(9): 76

9 Shi Q Y, Huo J J, Zheng Y R *et al*. *Materials Science and Engineering A*[J], 2018, 725: 148

10 Xia W S, Zhao X B, Yue L *et al*. *Journal of Alloys and Compounds*[J], 2020, 819: 152 954

11 Huo J J, Shi Q Y, Tin S *et al*. *Metallurgical and Materials Transactions A*[J], 2018, 49(11): 5298

12 Cervellon A, Hémery S, Kürnsteiner P *et al*. *Acta Materialia*[J], 2020, 188: 131

13 Wang X G, Liu J L, Jin T *et al*. *Materials and Design*[J], 2014, 67: 543

14 Cui L Q, Yu J J, Liu J L *et al*. *Materials Science and Engineering A*[J], 2018, 710: 309

15 Ru Y, Zhao H G, Zhang H *et al*. *Materials and Design*[J], 2019, 183: 108 082
16 Xu K, Wang G L, Liu J D *et al*. *Materials Science and Engineering A*[J], 2020, 786: 139 414
17 Benz J K, Carroll L J, Wright J K *et al*. *Metallurgical and Materials Transactions A*[J], 2014, 45(7): 3010
18 Tang Y L, Huang M, Xiong J C *et al*. *Acta Materialia*[J], 2017, 126: 336
19 Beyerlein I J, Hunter A. *Philosophical Transactions of the Royal Society A: Mathematical, Physical and Engineering Sciences*[J], 2016, 374(2066): 20 150 166
20 Carroll L J, Feng Q, Pollock T M. *Metallurgical and Materials Transactions A*[J], 2008, 39(6): 1290
21 Gao Q, Liu L R, Tang X H *et al*. *China Foundry*[J], 2019, 16(1): 14
22 Tian S G, Zhou H H, Zhang J H *et al*. *Materials Science and Engineering A*[J], 2000, 279(1-2): 160
23 Wang X G, Liu J L, Jin T *et al*. *Materials and Design*[J], 2015, 67: 543
24 Xu K, Wang G L, Liu J D *et al*. *Materials Science and Engineering A*[J], 2020, 786: 139 414
25 Miura N, Kurita K, Hayashi Y *et al*. *ISIJ International*[J], 2011, 51(4): 663

镍基单晶合金高温蠕变变形与损伤行为

闫化锦[1,3]，田素贵[2]，董志峰[1]
(1. 中国矿业大学(北京）机电与信息工程学院，北京 100083)
(2. 沈阳工业大学 材料科学与工程学院，辽宁 沈阳 110870)
(3. 贵州工程应用技术学院 机械工程学院，贵州 毕节 551700)

摘　要：通过蠕变性能测试和组织观察，研究了镍基单晶合金在高温蠕变期间的变形和损伤行为。结果表明，该合金在1040 ℃/137 MPa条件下的蠕变寿命为556 h，表现出优异的蠕变抗力。合金在稳态期间的蠕变特性是位错在γ基体中滑移和攀移越过筏状γ'相。在蠕变后期，合金的变形特征是位错剪切进入筏状γ'相，剪切γ'相的位错可以交滑移，形成的Kear-Wilsdorf（K-W）锁可抑制位错的滑移和交滑移。位错的交滑移能够促使筏状γ/γ'两相的扭曲，致使沿γ/γ'界面的裂纹萌生及界面断裂，这是合金的损伤和断裂特征。而$\sigma>\eta/\alpha$被认为是裂纹发生失稳扩展的条件。

关键词：镍基单晶合金；组织结构；蠕变；变形机制；损伤特征

作者简介：闫化锦，男，1984年生，博士，中国矿业大学（北京）机电与信息工程学院，北京 100083，电话：010-62331370，E-mail：yanhuajin317@163.com